RSC Advances

PAPER

View Article Online
View Journal | View Issue

Cite this: *RSC Adv.*, 2016, **6**, 1268

ESIPT blocked CHEF based differential dual sensor for Zn^{2+} and Al^{3+}in a pseudo-aqueous medium with intracellular bio-imaging applications and computational studies†

Rabiul Alam,[a] Tarun Mistri,[a] Rahul Bhowmick,[a] Atul Katarkar,[b] Keya Chaudhuri[b] and Mahammad Ali*[a]

Received 10th September 2015
Accepted 1st December 2015

DOI: 10.1039/c5ra18424j

www.rsc.org/advances

A novel 3-hydroxymethyl-5-methylsalicylaldehydenaphthyl-hydrazone (**H_3SAL-NH**) exhibits ESIPT behaviour due to proton transfer from the phenolic OH group to the azomethine N atom in the excited state. Through this ESIPT behaviour together with *cis–trans* isomerization of the azomethine group, the free ligand becomes very weakly fluorescent. However, in the presence of Zn^{2+} and Al^{3+} the ESIPT and isomerization are blocked due to coordination to the metal ions thereby causing turn on fluorescence for Al^{3+} and Zn^{2+}. Moreover, Zn^{2+} can easily be displaced from the [**H_2SAL-NH**–Zn^{2+}] complex by Al^{3+} thereby enhancing the differential selectivity for Al^{3+} over Zn^{2+}. This probe was found to be selective for Al^{3+} over Zn^{2+} in the presence of Na_2H_2EDTA, under both intra- and extracellular conditions. The LODs for Zn^{2+} and Al^{3+} were determined by 3σ methods and were found to be 3.1 nM and 0.92 nM, respectively. Thus, the differentially selective turn-on fluorescence behaviour of **H_3SAL-NH** for Zn^{2+} and Al^{3+} is based on the combined blocking of ESIPT and C=N isomerization, and a chelation-enhanced fluorescence (CHEF) effect. The coordination modes of the complexes were investigated through spectroscopic and computational studies. **H_3SAL-NH** also exhibits good photostability and very low cytotoxicity and is useful for fluorescence imaging of Zn^{2+} and Al^{3+} ions in live HepG2 cells.

Introduction

Molecular sensors are highly valuable tools for the selective recognition of chemical and biological species.[1] Though analyte selective molecular sensors are plentiful in the literature, probes with differential responses towards multiple analytes are highly desirable from the viewpoint of practical applications and are at the same time a challenge.[2,3]

Aluminium is a nonessential element, found in the +3 oxidation state in most kinds of animal and plant tissues and in natural waters everywhere.[4–8] It has been shown clearly that aluminium accumulates in various mammalian tissues such as the brain, bone, liver and kidney[9,10] which is accompanied by renal failure[11] and associated with age.[12]

According to a WHO report, the average daily human intake of aluminium is approximately 3–10 mg per day.[13] Thus the detection of Al^{3+} is attracting increasing interest in the areas of chemical, environmental and biological sciences, as the almost ubiquitous presence of this element has so heavily contaminated the environment that exposure to it is virtually inescapable.

However, compared to transition metals, the detection of Al^{3+} has always been a problematic task due to its lack of suitable spectroscopic characteristics and poor coordination ability[14] and as result only a few fluorescent chemosensors are available in the literature.[15]

On the other hand, Zn^{2+} plays an important role in various fundamental biological processes, such as gene transcription, regulation of metalloenzymes, neural signal transmission and apoptosis. However, elevated levels of Zn^{2+} in humans have been implicated in neurodegenerative disorders.[16,17]

A fluorescent probe is a molecular system that produces a detectable fluorescent signal upon interaction with a chemical species[18] and a number of signaling mechanisms like photo-induced electron/energy transfer (PET),[19] metal–ligand charge transfer (MLCT),[20] intramolecular charge transfer (ICT),[21] excimer/exciplex formation,[22] excited-state intra/intermolecular proton transfer (ESIPT),[23] and C=N isomerization have been developed and widely applied for the optical detection of different chemical species. As well as being good ligands for metal ions Schiff bases have antitumor,[24] anti-oxidant,[25] and attractive electronic and photophysical properties.[26]

[a]*Department of Chemistry Jadavpur University, Kolkata 700 032, India. E-mail: mali@chemistry.jdvu.ac.in; Fax: +91-33-2414-6223*

[b]*Molecular & Human Genetics Division, CSIR-Indian Institute of Chemical Biology, 4 Raja S.C. Mullick Road, Kolkata-700032, India*

† Electronic supplementary information (ESI) available. See DOI: 10.1039/c5ra18424j

In this paper, a 3-hydroxymethyl-5-methylsalicylaldehyde-naphthylhydrazone based Schiff base (**H_3SAL-NH**) was found to be poorly fluorescent, in part due to isomerization through rotation around the C=N double bond in the excited state[27] and in part due to ESIPT involving the phenolic proton and the imine nitrogen of the ligand.[28] We reasonably anticipate that the ESIPT and C=N isomerization may be inhibited upon complexation with a metal ion which will render selective detection through spectral (UV-vis and/or fluorescence) changes.

Experimental section

Materials and methods

The starting materials 3-hydroxy-2-naphthyl hydrazide (Sigma-Aldrich) and 2-hydroxy-3-hydroxymethyl-5-methylbenzaldehyde (prepared in this laboratory) were used for the preparation of the ligands. $Zn(NO_3)_2 \cdot 6H_2O$ (Merck, Germany) and $Al(NO_3)_3 \cdot 9H_2O$ (Merck, Germany) were used to prepare Zn^{2+} and Al^{3+} complexes. The solvents, ethanol, diethyl ether and tetrahydrofuran (THF) (Merck, India), were of reagent grade and were dried before use.

Physical measurements

Elemental analyses were carried out using a Perkin-Elmer 240 elemental analyser. Infrared spectra (400–4000 cm^{-1}) were recorded from KBr pellets on a Nicolet Magna IR 750 Series-II FTIR spectrometer. ^{1}H-NMR was recorded in DMSO-d_6 on a Bruker 300 MHz NMR spectrometer using tetramethylsilane ($\delta = 0$) as the internal standard. Lifetimes were measured in Horiba–Jobin–Yvon on a Hamamatsu MCP photomultiplier (R3809) and analysed using IBH DAS6 software. The pH of the solutions was recorded using a Systronics digital pH meter (Model 335, India) with the pH range 2–12. The pH meter was calibrated using standard buffer solutions (Acros Organics) of pH 4.0, 7.0 and 10.0. UV-vis spectra were recorded on an Agilent diode-array spectrophotometer (model: Agilent 8453) and steady-state fluorescence spectra were recorded on a Shimadzu spectrofluorimeter (model: RF-5301). ESI-MS$^+$ (m/z) of the ligand and Zn(II)-complex were recorded on a Waters HRMS spectrometer (model: XEVOG2 QTOF).

Solution preparation for UV-vis and fluorescence studies

For both UV-vis and fluorescence titrations, a stock solution of 1.0×10^{-3} M of the probe **H_3SAL-NH** was prepared in THF. Similarly, 1.0×10^{-3} M stock solutions of the metal ions $Al(NO_3)_3 \cdot 9H_2O$ and $Zn(NO_3)_2 \cdot 6H_2O$ and other metal ions were prepared in THF : H_2O (6 : 4). A buffer solution in THF : H_2O (3 : 2, v/v) containing 10.0 mM HEPES and 10 mM LiCl was prepared and the pH was adjusted to 7.20 using dilute HCl and NaOH solutions. 2.5 ml of this solution was pipetted into the cuvette to which was added 20 μL of the probe and metal ions incrementally starting from 0 to 60 μL in a regular interval of volume and the UV-vis and fluorescence spectra were recorded for each solution.

Job plot

This method is based on the measurement of a series of solutions in which the molar concentrations of the two reactants vary but their sum remains constant. The absorbance of each solution was measured at 398 nm for Al^{3+} and at 414 nm for Zn^{2+} and plotted against the mole fraction of one reactant. A maximum in absorbance occurs at the mole ratio corresponding to the combining ratio of the reactants. The composition of the complex was determined by Job's method and found to be (1 : 1) with respect to the ligand for both the Al^{3+} and Zn^{2+} complexes.

The preparation of 3-hydroxymethyl-5-methylsalicylaldehyde-naphthylhydrazone (H_3SAL-NH)

2-(Hydroxymethyl)-6-carbaldehyde-4-methylphenol was prepared according to the reported method.[29] 3-Hydroxy-2-naphthyl hydrazide (0.202 g, 1.0 mmol) was dissolved in 5 ml dry THF. To this solution, an ethanolic solution of 2-(hydroxymethyl)-6-carbaldehyde-4-methylphenol (0.166 g, 1.0 mmol) was added dropwise with continuous stirring. The resultant mixture was stirred for another 1 h maintaining a constant temperature at 40 °C. After the reaction was over, the white solid product was filtered and washed with cold diethyl ether and dried in air, then further recrystallized from EtOH (84% yield). Mp. 131 °C.

CHN analysis for $C_{20}H_{18}N_2O_4$: calculated (%): C, 68.56; H, 5.18; N, 8.00. Found (%): C, 68.54; H, 5.16; N, 7.97. ^{1}H-NMR (in DMSO-d_6) (δ, ppm): 2.27 (s, 3H); 4.56 (d, $J = 4.9$, 2H); 5.08 (t, $J = 5.4$, 1H); 7.14 (s, 1H); 7.26 (s, 1H); 7.35 (m, 1H); 7.51 (t, $J = 7.6$, 1H); 7.56 (d, $J = 8.2$, 1H); 7.91 (d, $J = 8.1$); 8.44 (s, 1H); 8.57 (s, 1H); 11.04 (s, 1H); 11.62 (s, 1H); 12.21 (s, 1H, NH), (please see Fig. S1† for the ^{1}H-NMR spectrum). ^{13}C-NMR: (75 MHz, DMSO-d_6) δ_{ppm}: 20.60, 58.09, 111.07, 117.31, 120.45, 124.33, 126.32, 127.26, 127.92, 128.80, 129.15, 129.51, 130.08, 130.71, 130.91, 136.40, 151.08, 153.05, 154.37, 163.88 (Fig. S2†). ESI-MS$^+$ (m/z): 373.1164 (**H_3SAL-NH** + Na^+) (Fig. S3†).

Complex 1. $Al(NO_3)_3 \cdot 9H_2O$ (0.375 g, 1 mmol) was dissolved in 10 ml of a THF : ethanol mixture (2 : 8, v/v) and to this solution the ligand **H_3SAL-NH** (0.350 g, 1.0 mmol) in 3 ml THF was added. The color of the solution changed to yellow. The resulting mixture was stirred for 3 h. The volume of the solution was reduced to 5 ml under reduced pressure and diethyl ether (10 ml) was added. This was then kept at 0 °C for 12 h to afford complex **1** as a crystalline material. Yield: 0.356 g (~52%). UV-vis (THF): λ_{max} 398 nm (Fig. S4†). CHN analyses for [Al(SAL-NH)(OH_2)]: $C_{20}H_{17}N_2O_5Al$ (MW 392.34), calcd (%): C, 61.23; H 4.37; N, 7.14. Found (%): C, 61.29, H, 4.39, N, 7.10.

Complex 2. $Zn(NO_3)_2 \cdot 6H_2O$ (0.297 g 1.0 mmol) was dissolved in 10 ml of a THF : ethanol mixture (2 : 8, v/v) and to this solution, **H_3SAL-NH** (0.350 g, 1.0 mmol) in 3 ml THF was added. The color of the solution changed to bright yellow. The resulting mixture was stirred for 3 h. The volume of the solution was then reduced to 5 ml under reduced pressure and diethyl ether (10 ml) was added. This was then kept at 0 °C for 12 h to afford complex **2** as a crystalline material. Several trials to get single crystals were not successful. Yield: 0.398 g (~70%). UV-vis

(THF): λ_{max}, 414 nm (Fig. 1). CHN analyses for [Zn(**H_2SAL-NH**)(OH)]: $C_{20}H_{18}N_2O_5Zn$ (MW 430.05), calcd (%): C, 55.64; H 4.20; N, 6.49. Found (%): C, 55.69, H, 4.23, N, 6.38.

Computational details

Ground state electronic structure calculations in a THF solution of the ligand and complexes have been carried out using DFT[30] associated with the conductor-like polarizable continuum model (CPCM).[31] Becke's hybrid function[32] with the Lee–Yang–Parr (LYP) correlation function[33] was used throughout the study. The geometries of the ligand and complexes were fully optimized in the solution phase without any symmetry constraints. On the basis of the optimized ground state geometry, the absorption spectral properties in a THF medium were calculated by time-dependent density functional theory (TDDFT)[34] associated with the conductor-like polarizable continuum model. We computed the lowest 40 singlet–singlet transitions and the results of the (TD) calculations were qualitatively very similar. The TDDFT (B3LYP) approach, a reliable method for calculating the spectral properties of many transition metal complexes,[35] has been adopted to get more accurate electronic excitation energies.

The effective core potential (ECP) approximation of Hay and Wadt was used to describe the core electrons for both aluminium and zinc whereas the associated "double-ξ" quality basis sets were used for the valence shell.[36] For H atoms we used the 6-31(g) basis set; for C, N and O atoms we employed 6-31+g as the basis set for all the calculations. The calculated electron density plots for the frontier molecular orbitals were prepared by using Gauss View 5.1 software. All the calculations were performed with the Gaussian 09W software package.[37] The GaussSum 2.1 program[38] was used to calculate the molecular orbital contributions from groups or atoms.

Cell culture

HepG2 cell line human hepatocellular liver carcinoma cells, were procured from the National Center for Cell Science, Pune, India, and used throughout the study. The cells were cultured in DMEM (Gibco BRL) supplemented with 10% FBS (Gibco BRL) and a 1% antibiotic mixture containing penicillin, streptomycin and gentamicin (Gibco BRL) at 37 °C in a humidified incubator with 5% CO_2. The cells were grown to 90% confluence, harvested with 0.025% trypsin (Gibco BRL) and 0.52 mM EDTA (Gibco BRL) in phosphate-buffered saline (PBS). The 35 mm plated was seeded in such way as to get a 60–70% confluent cell population for treatment after incubation.

Cell cytotoxicity assay

To test the cytotoxicity of **H_3SAL-NH** an assay was performed as per the procedure described earlier.[39] After treatment with **H_3SAL-NH** at different doses of 1, 10, 20, 50 and 100 μM, respectively, for 12 h, 10 μl of MTT solution (10 mg ml^{-1} PBS) was added to each well of a 96-well culture plate and this was again incubated continuously at 37 °C for a period of 3 h. All

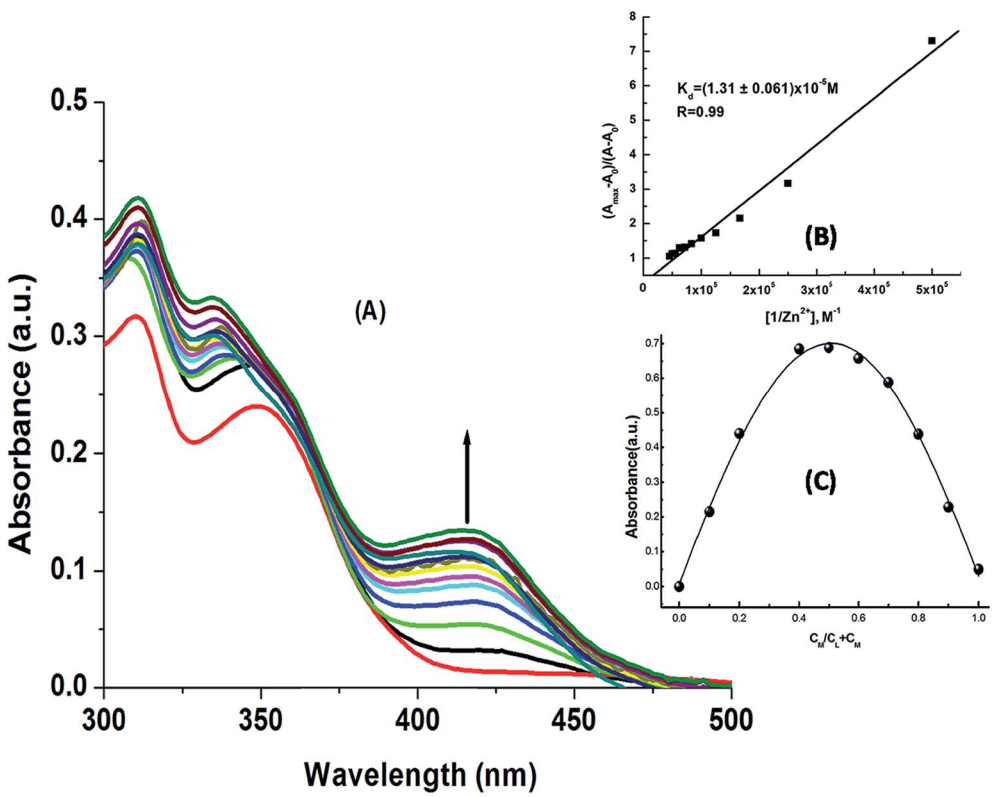

Fig. 1 (A) Absorption titration spectra of **H_3SAL-NH** with $Zn(NO_3)_2 \cdot 6H_2O$ in HEPES buffer (10 mM) at pH 7.2 recorded in THF : H_2O (6 : 4, v/v); (B) Benesi–Hildebrand plot; (C) Job plot at 414 nm.

media were removed from the wells and 100 μl acidic isopropyl alcohol was added into each well. The intracellular formazan crystals (blue-violet) formed were solubilized with 0.04 N acidic isopropyl alcohol and the absorbance of the solution was measured at 595 nm with a microplate reader (model: Thermo Scientific Multiskan EX). The cell viability was expressed as the optical density ratio of the treated cells to the control. Values are expressed as the mean ± standard error of three independent experiments. The cell cytotoxicity was calculated as % cell cytotoxicity = 100% − % cell viability.

Cell imaging study

HepG2 cells were incubated with 10 μM **H_3SAL-NH**. The stock solution (1 mM) was prepared by dissolving **H_3SAL-NH** in a mixed solvent (DMSO : water = 1 : 9 (v/v)) in the culture medium followed by incubation for 30 min at 37 °C. After incubation, the cells were washed twice with phosphate-buffered saline (PBS). Bright field and fluorescence images of the HepG2 cells were taken using a fluorescence microscope (Leica DM3000, Germany) with an objective lens of 40× magnification.

Results and discussion

UV-vis absorption studies

The electronic absorption properties of (**H_3SAL-NH**) were investigated in THF : H_2O (6 : 4, v/v) and HEPES buffer (10 mM) at pH 7.2. The band at 349 nm is assigned to the electronic transition involving the HO–C=C–C=N chromophore in the enol form.[40–43] The band at 313 nm is attributed to the azomethine C=N group.

It was anticipated that the nitrogen of the –C=N bond would take part in the coordination with Zn^{2+} to form a **H_2SAL-NH**–Zn^{2+} complex, thereby inhibiting the ESIPT (Scheme 1). Moreover, new absorption bands appear at 398 nm for Al^{3+} and at 414 nm for Zn^{2+}, which is probably caused by an intraligand charge transfer (ILCT) transition of the $\pi \rightarrow \pi^*$ type, which is certainly caused by a larger conjugation in the ligand system.

The absorption titration spectra for a fixed concentration of **H_3SAL-NH** (20 μM) and a variable concentration of Zn^{2+} and Al^{3+} (0 to 26 μM) are shown in Fig. 1 and S4.† There is a gradual increase in the absorbance at 398 nm for Al^{3+} and 414 for Zn^{2+} with the increase in metal ion concentration, reaching a maximum at ~1 : 1 metal to ligand concentration and then becoming saturated (Fig. 1A). All these data were fitted to the Benesi–Hildebrand equation to get the dissociation constant and stoichiometry of complexation.

$$\frac{(A_{max} - A_0)}{(A - A_0)} = 1 + \frac{1}{K_d[M]^n}$$

where, A_0 and A_{max} are the absorbance of the pure ligand in the absence of the metal ion and in the presence of excess metal ions, respectively. A linear least square fit of $(A_{max} - A_0)/(A - A_0)$ against 1/[M] clearly demonstrates $n = 1$, indicating a 1 : 1 complexation for both the metal ions. The linear fit also gives the apparent dissociation constants of the complexes as $K_d = (7.17 \pm 0.18) \times 10^{-6}$ M for Al^{3+} and $K_d = (1.31 \pm 0.06) \times 10^{-5}$ M, for Zn^{2+}. The 1 : 1 L : M binding was further determined by Job's method (Fig. 1C and S4†).

Fluorescence studies

In order to check the selectivity of the probe **H_3SAL-NH** for Zn^{2+} and Al^{3+} detection we have carried out fluorescence experiments

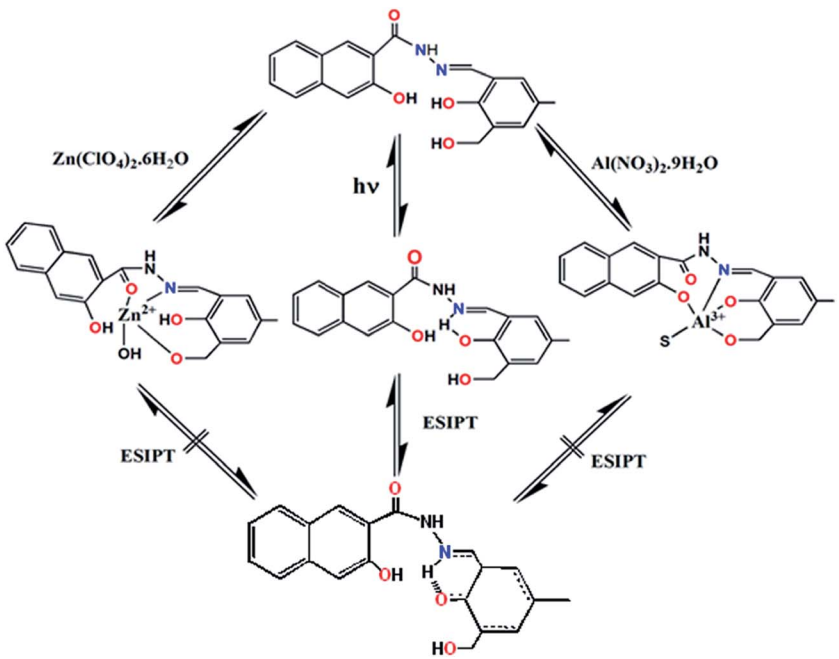

Scheme 1 Proposed ESIPT in the compound H_3SAL-NH (1).

with 20 μM **H_2SAL-NH** and 5 equivalents of different metal ions. It was interesting to note that the detection of Al^{3+} was not perturbed by biologically abundant Na^+, K^+, Ca^{2+}, *etc.*, metal ions. Several transition metal ions, namely Cr^{3+}, Zn^{2+}, Mn^{2+}, Fe^{2+}, Fe^{3+} and Hg^{2+}, also caused no interference (Fig. 2A). However, the detection of Zn^{2+} is affected by Al^{3+} only so in absence of Al^{3+} the probe can selectively recognize Zn^{2+}. In the presence of Zn^{2+} and Al^{3+} the probe is highly selective towards Al^{3+} only.

The emission spectra of **H_3SAL-NH** (20 μM) and its fluorescence titration with $Al(NO_3)_3 \cdot 9H_2O$ and $Zn(NO_3)_2 \cdot 6H_2O$ (recorded in THF : H_2O (6 : 4, v/v)) in HEPES buffer (10 mM) at pH 7.2 are shown in Fig. 3 and 4. The ligand itself is very weakly fluorescent, showing a weak band centred around 543 nm, due to ESIPT and C=N isomerization. However, on addition of Al^{3+} or Zn^{2+} the fluorescence intensity increases enormously, giving turn-on fluorescence responses with values ~30 fold higher for Al^{3+} at $\lambda_{em} = 486$ nm and ~18 fold higher for Zn^{2+} at $\lambda_{em} = 498$ nm with respect to the free ligand. In addition, there is a gradual blue shift of λ_{em} from 543 nm for the pure ligand to 486 nm and 498 nm on complexation with Al^{3+} and Zn^{2+} respectively, which is accompanied with a large increase in the fluorescence lifetime (τ) of **H_3SAL-NH** (Fig. S5 and S6†). Thus, τ (0.0067 ns) for the free ligand (**H_3SAL-NH**) increases enormously [τ(**SAL-NH-Al**) = 5.04 ns (757 fold) and τ[**H_2SAL-NH**–Zn(OH)] = 3.2 ns (477 fold)] in the presence of 1.2 equivalents of the respective metal ions. The Benesi–Hildebrand equation was employed to analyze the fluorescence titration data to get the apparent dissociation constant values and the evaluated parameters are: $K_d = (3.14 \pm 0.08) \times 10^{-6}$ M for Al^{3+} and $K_d = (1.12 \pm 0.04) \times 10^{-5}$ M for Zn^{2+}. It should be mentioned here that the K_d values evaluated from the absorbance and fluorescence titration data are in excellent agreement manifesting the self-consistency of our experimental results.

In the UV-vis spectrum of the free ligand, the absorption peak at 349 nm is assigned to the HO–C=C–C=N chromophore. When we generate the excitation spectrum of the ligand keeping the emission wavelength fixed at 557 nm, two excitation peaks appear at λ_{max} 348 and 460 nm manifesting the existence

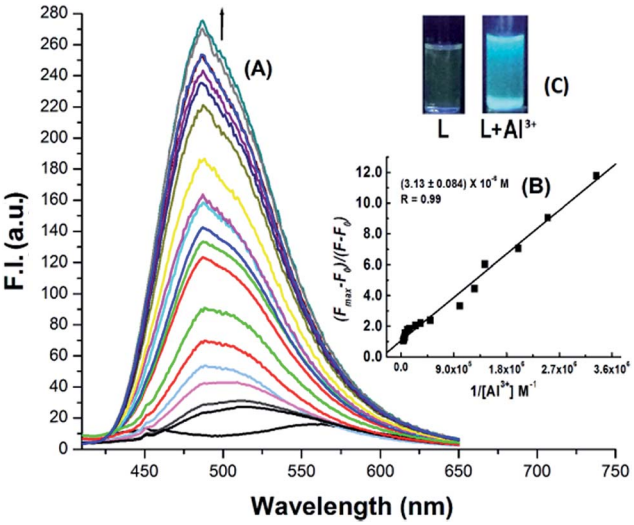

Fig. 3 (A) Fluorescence titration of H_3SAL-NH (20 μM) in HEPES buffer at pH 7.2 recorded in THF : H_2O (6 : 4, v/v) with the gradual addition of Al^{3+} with $\lambda_{ex} = 398$ nm and $\lambda_{em} = 486$ nm. Inset (B) B–H plot of F.I. *vs.* 1/[Al^{3+}]; (C) UV-exposed image of H_3SAL-NH with Al^{3+}.

of both the enol and keto forms, the latter being assigned to the keto form, which arises due to the intramolecular proton transfer from the phenolic OH to the azomethine N resulting in C=O and –C–NH and thus increasing the conjugation (Fig. S7†). **H_3SAL-NH** is poorly fluorescent, partly due to isomerization around the C=N double bond (Scheme 2) and partly due to the intramolecular proton transfer in the excited state (ESIPT). Upon stable chelation with Al^{3+} or Zn^{2+}, the C=N isomerization as well as the ESIPT are blocked (Scheme 1), leading to the increase in fluorescence intensity by chelation enhanced fluorescence (CHEF) effects.[44]

Selectivity studies

Next, the selectivity of Al^{3+} over Zn^{2+} was examined by the addition of 1 equivalent of Al^{3+} to the [**H_2SAL-NH**–Zn^{2+}] ensemble (Fig. 5) which showed an instantaneous decrease in

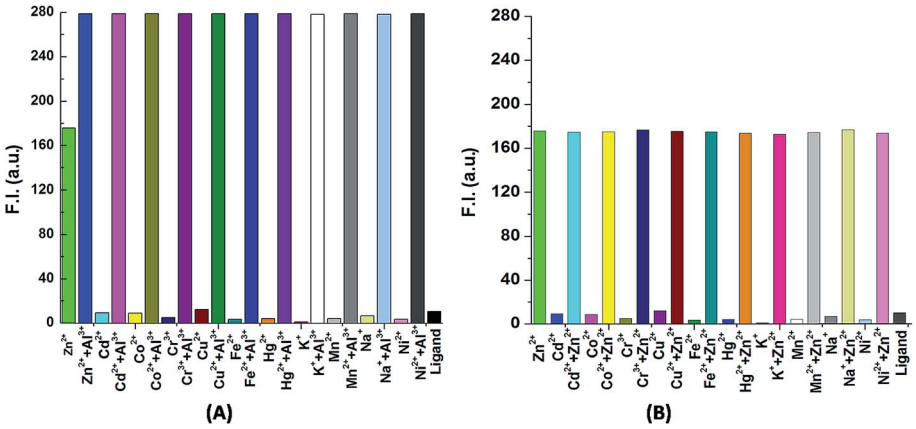

Fig. 2 (A) Histogram plot for the detection of Al^{3+} with different ions. (B) Histogram plot for the detection of Zn^{2+} in absence of Al^{3+} and with different ions.

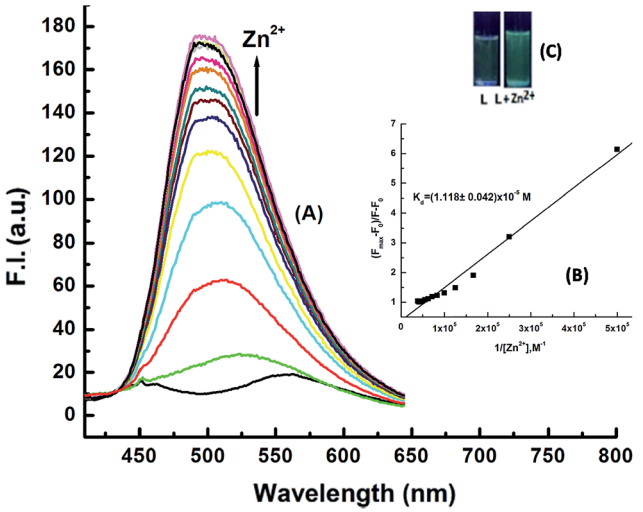

Fig. 4 (A) Fluorescence titration of H_3SAL-NH (20 μM) in HEPES buffer at pH 7.2 recorded in THF : H_2O (6 : 4, v/v) with the gradual addition $Zn(NO_3)_2 \cdot 6H_2O$ with $\lambda_{ex} = 398$ nm and $\lambda_{em} = 498$ nm. (B) B–H plot of F.I. *vs.* $1/[Zn^{2+}]$; (C) UV-exposed emission image of H_3SAL-NH with Zn^{2+}.

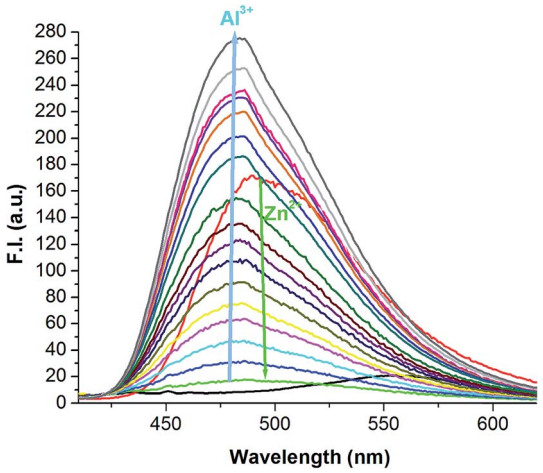

Fig. 5 Selectivity for Al^{3+} over the H_2SAL-NH–Zn^{2+} complex.

the emission intensity at 498 nm due to the formation of an [Al^{3+}–**H_2SAL-NH**–Zn^{2+}] intermediate and then a gradual increase at 486 nm with time, clearly indicating the displacement of Zn^{2+} by Al^{3+}. This also indicates a slow uptake of Al^{3+} by the receptor manifesting the fact that this complexation is kinetically slow but the formed complex is thermodynamically stable over the **H_2SAL-NH**–Zn^{2+} complex. Therefore, all the UV-vis and fluorescence spectra of the SAL-NH–Al^{3+} titrations were taken after half an hour of mixing the guest with the host molecule. However, when we used [**SAL-NH**–Al^{3+}] and added an excess (2 to 100 equivalents) of Zn^{2+}, we did not see any change in the spectral pattern (Fig. S8†). Thus the probe is highly selective towards only Al^{3+} even in the presence of Zn^{2+} [Fig. 2 and 5]. The ligand is also selective towards Zn^{2+} in the presence of other metal ions but in the absence of Al^{3+} [(Fig. 2)]. However, Na_2H_2EDTA extracts Zn^{2+} from the **H_2SAL-NH**–Zn^{2+} complex as $[ZnEDTA]^{2-}$, thereby masking the fluorescence of the Zn–probe complex (Fig. 2), but Na_2H_2EDTA has no such effect on the [**SAL-NH**–Al^{3+}] complex. Thus the probe is highly selective for Al^{3+} even in presence of excess Zn^{2+} ions (Fig. S9†).

The limits of detection (LODs) for Zn^{2+} and Al^{3+} were determined by 3σ methods which are found to be 3.1 nM and 0.92 nM, respectively (Fig. S10†). In the presence of 1 equivalent of Zn^{2+} and Na_2H_2EDTA the LOD of Al^{3+} for the [**SAL-NH**–Al^{3+}] complex was calculated to be 3.2 nM (Fig. S10c†). The quantum yields of the Zn^{2+} and Al^{3+} complexes of **H_3SAL-NH** were determined to be 0.062 (Zn complex) and 0.0705 (Al complex), which are respectively 21 and 23 times higher than that of the pure ligand (0.003).

Different spectroscopic techniques were adopted to establish the mode of coordination of the **H_3SAL-NH** probe towards Al^{3+} and Zn^{2+} ions in solution. The mass spectrum of [M(**SAL-NH**)] in THF revealed that **H_3SAL-NH** : M = 1 : 1 with ESI-MS^+ (m/z) = 437.20 for ([Zn(**H_2SAL-NH**)(OH)] + Li^+) and ESI MS^+ (m/z) = 407.17 for [Al(**SAL-NH**)(CH_3OH) + H^+] (Fig. S3a and b†). A comparison of the FTIR spectra of the free **H_3SAL-NH** and its complexes revealed a shift in $\nu_{C=N}$ from 1643 cm^{-1} for the free ligand to 1621 and 1635 cm^{-1} for the Zn^{2+} and Al^{3+} complexes, respectively indicating a significant binding between them (Fig. S11†).

The coordination modes were further supported by ^{1}H-NMR studies (Fig. 6) which clearly showed a change in the chemical shifts of the azomethine proton of the free ligand from 8.57 ppm to 8.64 and 8.59 ppm in presence of 1 equivalent of Al^{3+} and Zn^{2+} respectively (Table S1†). The OH proton on the hydroxymethyl group of the free ligand vanishes due to its strong participation in bonding with Zn^{2+} but the other OH protons and the –NH proton remain unchanged due to their non-participating behavior but in the case of Al^{3+} all three OH protons vanish with the addition of 1 equivalent Al^{3+}. This

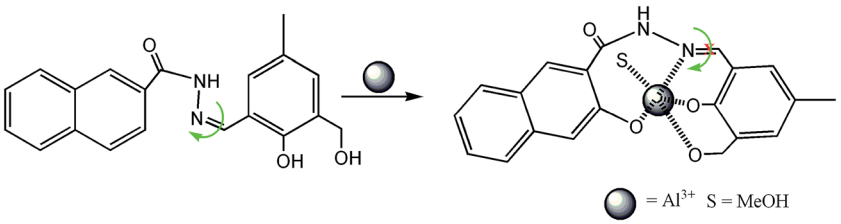

Scheme 2 C=N isomerization.

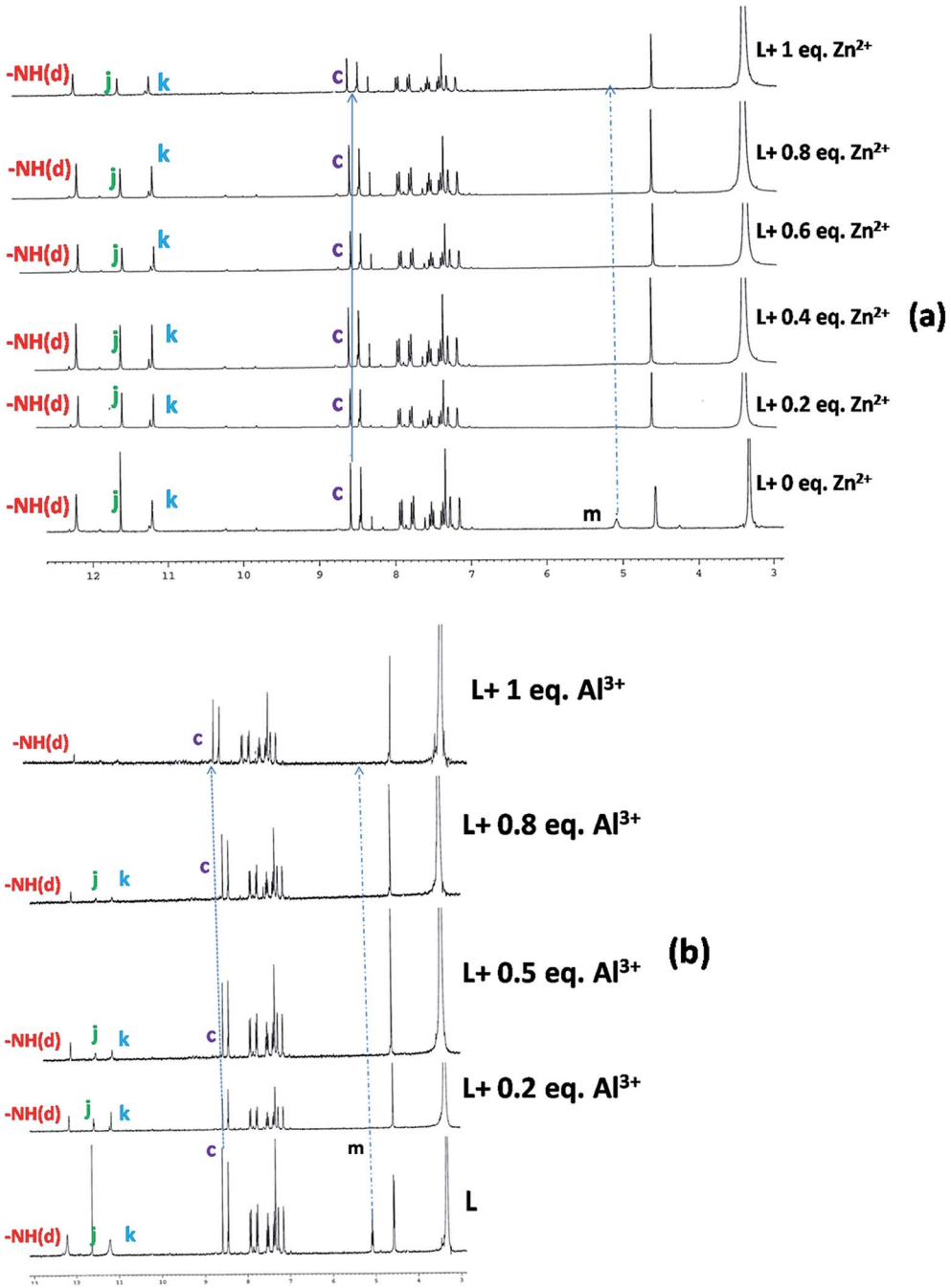

Fig. 6 ^{1}H-NMR titration of the free ligand (L = **H_3SAL-NH**) and with the addition of 1 equivalent of Zn^{2+} (a) and Al^{3+} (b) in DMSO-d_6 recorded on a 300 MHz Bruker NMR spectrometer.

clearly signifies that the OH protons are engaged in binding with Al^{3+} but there is no shift of the –NH proton which suggests its non-participation in bonding with metal ions.

Thus, we can conclude that two phenolate O atoms and one imine N atom and hydroxymethyl group of **H_3SAL-NH** are involved in binding with Al^{3+} but in case of the Zn^{2+} hydroxymethyl group, one imine N atom the hydroxo and amido O atoms are involved in binding but the two phenolate O atoms are not involved in binding. This was further supported by detailed DFT calculations on the free ligand and its Al^{3+} and Zn^{2+} complexes (*vide infra*). The non-participation of the phenoxo O41 and naphthoxo O17 in bonding with the Zn atom comes from the fact that they are not within bonding distance [Zn44–O41 = 2.93 Å and Zn44–O41 = 5.54 Å].

The binding affinity of the probe is greater for Al^{3+} than Zn^{2+} as evidenced from the formation constant values ($K_{Al}{}^{3+} = 3.18 \times 10^5$ M^{-1} and $K_{Zn}{}^{2+} = 8.93 \times 10^4$ M^{-1}) and thus displacement of the latter by Al^{3+} can be explained by the fact that the present probe provides comparatively hard donor atoms for the hard acid Al^{3+}.

Geometry optimization and electronic structure

The optimized geometries of **H_3SAL-NH** and its Zn^{2+} and Al^{3+} complexes are shown in Fig. 7. The compositions of the complexes as [Al(**SAL-NH**)(MeOH)] and [[Zn(**H_2SAL-NH**)(OH)] were adopted based on HRMS studies which indicated the presence of one MeOH and one hydroxyl group in their molecular fragments. **H_3SAL-NH**, and **SAL-NH**–Al^{3+} (**1**) and **H_2SAL-NH**–Zn^{2+} (**2**) complexes have the C1 point group. The important optimized geometrical parameters of the complexes are listed in Table S2.†

In the case of complex **1** the Al^{3+} center adopts a trigonal bipyramidal geometry. The calculated Al–N bond distance is 2.107 Å and the Al–O bond distance fall in the range 1.806–1.998 Å. Here the equatorial sites are occupied by one phenoxo oxygen (O48) one imime nitrogen (N4) and the oxygen (O22) of the hydroxymethyl group, while the axial sites are occupied by a phenoxo oxygen (O48) and an oxygen atom (O30) of the MeOH solvent. In the case of complex **2** the Zn^{2+} centre is tetra-coordinated where all the Zn–O bond distances span the range 1.841–2.128 Å and the Zn–N distance is 2.247 Å.

In the case of **H_3SAL-NH** in the ground state, the electron density of the HOMO and HOMO−2 orbitals resides mainly on the phenyl ring and the phenoxo oxygen attached to the naphthyl moiety, whereas for the HOMO−3 orbital it remains at the naphthyl ring and for the HOMO−4 orbital it is at the imine nitrogen atom. The energy gap between the HOMO and LUMO is 3.78 eV (Fig. 8). In the case of the HOMO−3 orbital of complex **1** the electronic contribution comes mainly from the naphthyl moiety and in HOMO−2 it comes from the phenyl moiety. The HOMO–LUMO energy gap is 3.60 eV (Fig. 8). In the case of **2** the electronic contribution in the HOMO−5 and HOMO orbitals mainly originates from the phenyl moiety with a HOMO–LUMO energy gap of 3.09 eV (Fig. 8).

The UV-vis absorption spectra of the ligand used in the present work were calculated at room temperature in THF by the TDDFT method. The ligands show three well resolved peaks at 350, 313 and 302 nm and all have an ILCT character. These bands are assigned to the $S_0 \rightarrow S_4$, $S_0 \rightarrow S_{11}$ and $S_0 \rightarrow S_{12}$ electronic transitions, respectively (Fig. 9). The absorption energies associated with their oscillator strengths are given in Table 1 and S3.†

The UV-vis spectrum of the [Al(**SAL-NH**)(MeOH)] complex shows three absorption bands at 398, 335 and 321 nm in THF at room temperature which correspond nicely to the TDDFT calculated absorption bands located at 399, 341 and 314 nm

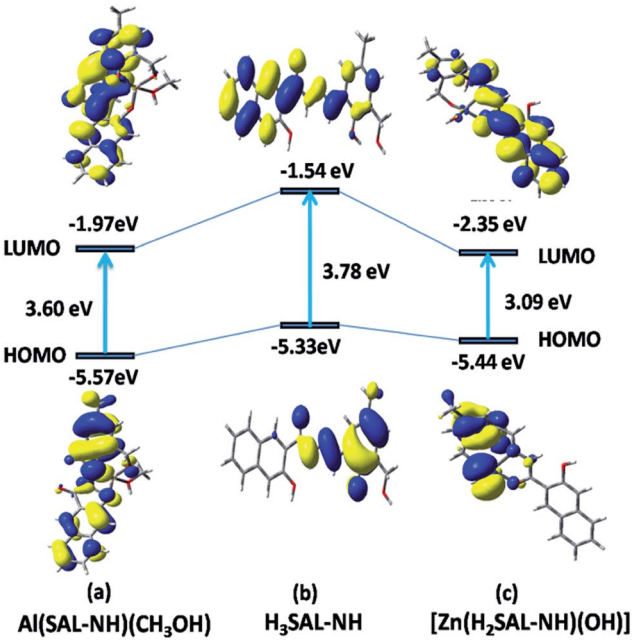

Fig. 8 Frontier molecular orbitals of H_3SAL-NH and its [Al(SAL-NH)(MeOH)] and [Zn(**H_2SAL-NH**)(OH)] complexes.

(Fig. 10) (Table S4† and 1). These three absorption bands can be assigned to the $S_0 \rightarrow S_2$, $S_0 \rightarrow S_5$ and $S_0 \rightarrow S_6$ transitions, respectively (Fig. 10) originating from a mixture of MLCT and ILCT transitions (Table S4†).

The [Zn(**H_2SAL-NH**)(OH)] complex shows two absorption bands at 412 and 335 nm (Fig. S12†) and the corresponding calculated absorption bands are located at 420 and 333 nm which are in excellent agreement with the experimental results (Tables S5† and 1). These two absorption bands can be assigned to the $S_0 \rightarrow S_1$ and $S_0 \rightarrow S_6$ transitions respectively originating from a mixture of MLCT and ILCT transitions (Table S5†).

pH studies

The dependence of the fluorescence intensity of the free ligand and its Al^{3+} and Zn^{2+} complexes on the pH of the medium was investigated in the pH range 2.0 to 12.0 at [**H_3SAL-NH**] = 20 μM, [M^{n+}] = 30 μM in 6 : 4 THF : H_2O v/v in HEPES buffer. It was observed that in the pH range 3 to 8 the F. I. of the free ligand remains almost constant. However, on addition of 1.2 equivalents of Al^{3+} the F. I. jumps to 275 ± 10 and remains constant in

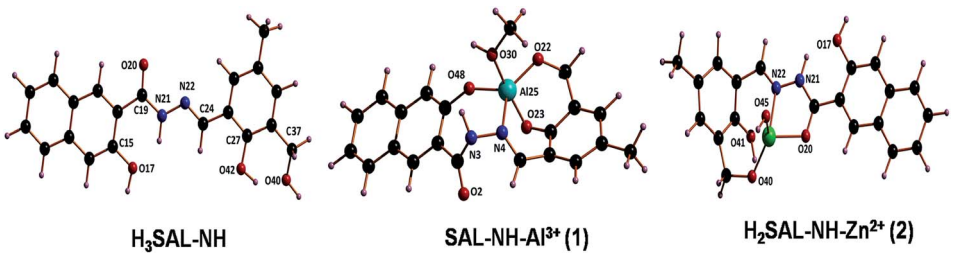

Fig. 7 Optimized molecular structures of the ligand, complex **1** and complex **2**.

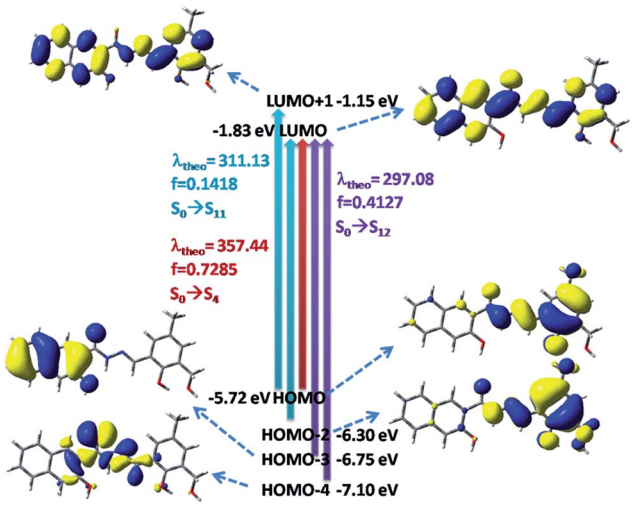

Fig. 9 Frontier molecular orbitals involved in the UV-vis absorption of H_3SAL-NH in THF solution.

Table 1 The comparable calculated optical transitions with experimental UV-vis values for the ligand (H_3SAL-NH), complex (1) and complex 2

Ligand and complex (3)	Theoretical (nm)	Experimental (nm)	Electronic transition	f
Ligand	357.44	350	$S_0 \rightarrow S_4$	0.7285
Ligand	311.13	313	$S_0 \rightarrow S_{11}$	0.1418
Ligand	297.08	303	$S_0 \rightarrow S_{12}$	0.4127
Complex **1**	399.63	398	$S_0 \rightarrow S_2$	0.0565
Complex **1**	341.53	335	$S_0 \rightarrow S_5$	0.0401
Complex **1**	314.55	321	$S_0 \rightarrow S_6$	0.2680
Complex **2**	420.42	412	$S_0 \rightarrow S_1$	0.1365
Complex **2**	332.69	335	$S_0 \rightarrow S_6$	0.4355

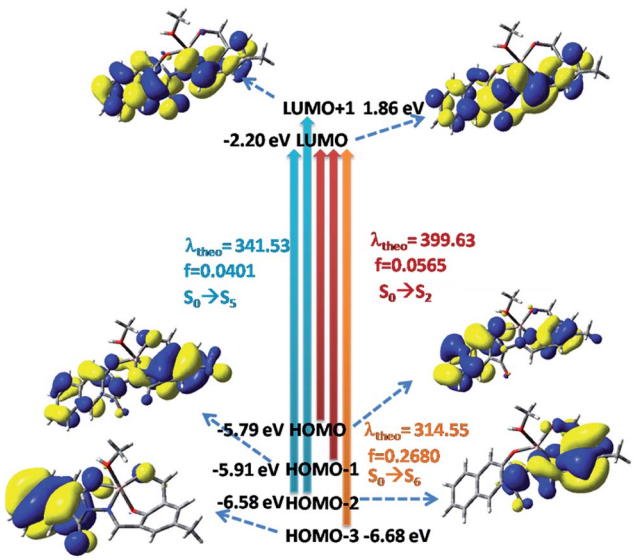

Fig. 10 Frontier molecular orbitals involved in the UV-vis absorption of complex 1.

the pH range 7–9, but on a further increase in pH the F. I. gradually falls. Similar is the trend in the case of the Zn^{2+} complex but here the F. I. remains almost constant at $\sim 179 \pm 10$ in the pH range 7–11 and then the F. I. gradually falls. All these are shown in Fig. 11.

Cell imaging experiments

Taking into consideration the excellent sensing performance of **H_3SAL-NH** for Al^{3+} and Zn^{2+}, we decided to utilize **H_3SAL-NH** for the fluorescence imaging of Al^{3+} and Zn^{2+} in living cells (Fig. 12). To determine whether **H_3SAL-NH** has any cytotoxic effect we have used HepG2 cells. **H_3SAL-NH** does not affect the cell viability, as confirmed by the MTT assay (Fig. S13†). There was no significant reduction in the tetrazolium salt, reflecting a decrease in formazan production for **H_3SAL-NH** up to 50 μM. More than 92% cell viability was observed for **H_3SAL-NH** at 10 μM after which the viability of the HepG2 cells decreases slightly (viability curve). Hence further experiments were carried out with 10 μM of **H_3SAL-NH**. The intracellular imaging of **H_3SAL-NH** on HepG2 cells under fluorescence microscopy displayed no or weak intracellular fluorescence when treated with 10 μM **H_3SAL-NH** (Fig. 12). An obvious fluorescence was observed inside the cells when the HepG2 cells were incubated with 10 μM **H_3SAL-NH** +10 μM Al^{3+} and 10 μM **H_3SAL-NH** +10 μM Zn^{2+} for 30 min at 37 °C. In order to validate the finding that Zn^{2+} and Al^{3+} bind with **H_3SAL-NH**, we have separately treated the HepG2 cells with 10 μM **H_3SAL-NH** +10 μM Al^{3+} and 10 μM **H_3SAL-NH** +10 μM Zn^{2+} for 30 min at 37 °C in another set of experiments followed by the addition of 100 μM Na_2H_2EDTA for another 30 min at 37 °C and fluorescence images were taken (Fig. 12). The HepG2 cells incubated with 10 μM **H_3SAL-NH** + 10 μM Zn^{2+} at 37 °C showed almost complete quenching of fluorescence due to the removal of Zn^{2+} from the **H_2SAL-NH**–Zn^{2+} complex by Na_2H_2EDTA, whereas there was no change in the fluorescence intensity after the addition of Na_2H_2EDTA to the **SAL-NH**–Al^{3+} complex (Fig. 12). This implies that the **SAL-NH**–Al^{3+} complex is more stable than the **H_2SAL-NH**–Zn^{2+} complex in the presence of Na_2H_2EDTA. We have presented a novel

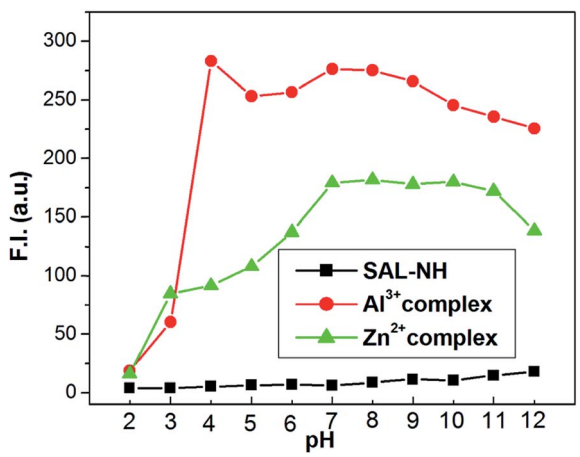

Fig. 11 pH dependence of fluorescence responses of H_3SAL-NH and its Zn^{2+} and Al^{3+}-complexes in 6 : 4 (v/v) THF/water in HEPES buffer.

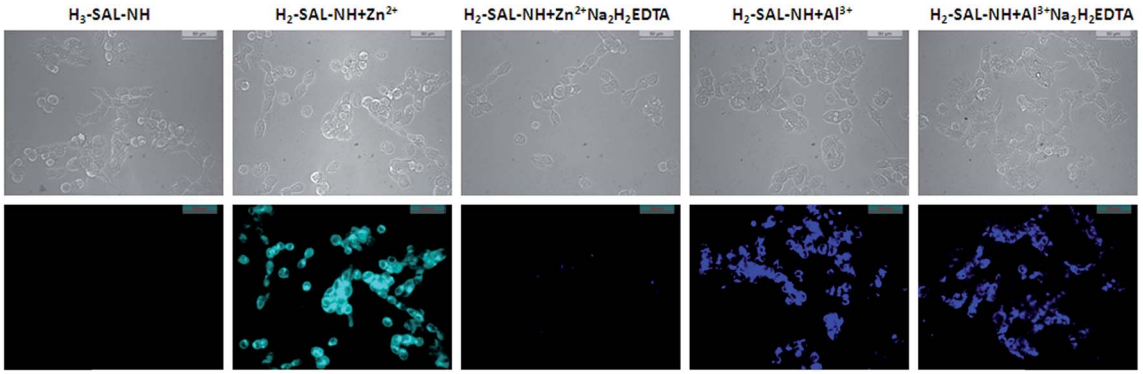

Fig. 12 The phase contrast and fluorescence images of HepG2 cells captured after incubation with H_3SAL-NH, H_3SAL-NH + Zn^{2+} and H_3SAL-NH + Al^{3+} for 30 min at 37 °C, followed by the addition of 100 μM Na_2H_2EDTA after the cells were pre-incubated with (H_3SAL-NH + Zn^{2+}) and (H_3SAL-NH + Al^{3+}) for 30 min at 37 °C.

fluoroionophore for sensing Zn^{2+} and Al^{3+} ions. **H_3SAL-NH** also exhibits good photostability and very low cytotoxicity. The fluorescence images of the live cells reveal that it can easily diffuse into the cell and can easily sense the Zn^{2+} and Al^{3+} ions by forming a stable complex at low concentrations. However, unlike the Zn^{2+} ion, Al^{3+} forms a stable complex with **H_3SAL-NH**, particularly with respect to the reaction with H_2EDTA^{2-}. This enhances the selectivity of the novel fluoroionophore for Al^{3+} over Zn^{2+}.

Conclusions

In summary, a novel 3-hydroxymethyl-5-methylsalicylaldehyde-naphthylhydrazone (**H_3SAL-NH**) fluoroionophore was synthesized and characterized by various spectroscopic techniques. Due to ESIPT behavior arising from proton transfer from the phenolic OH to the azomethine N atom in the excited state together with *cis–trans* isomerization along the C=N bond of the azomethine group, the free ligand becomes very weakly fluorescent. However, in the presence of selective metal ions like Zn^{2+} and Al^{3+} the ESIPT and isomerization are blocked through coordination to the metal ions, thereby exhibiting turn on fluorescence for Al^{3+} and Zn^{2+}. Moreover, Zn^{2+} can easily be displaced from the [**H_2SAL-NH**–Zn^{2+}] complex by Al^{3+} thereby enhancing the differential selectivity of Al^{3+} over Zn^{2+}. Not only that, this probe could be made selective towards Al^{3+} over Zn^{2+} in the presence of Na_2H_2EDTA. All these properties can conveniently be demonstrated both in *in vivo* and *in vitro* conditions. Fluorescence and UV-vis titrations at a fixed concentration of the probe and a variable metal ion concentration gives us the conditional dissociation constants (K_d) and hence the K'_f (formation constants) values which were found to be in excellent agreement for the two techniques. The 1 : 1 stoichiometry of the reaction between **H_3SAL-NH** and Al^{3+} and Zn^{2+} were determined by Job's method and were also in agreement with those obtained from the titration data. The LODs for Zn^{2+} and Al^{3+} were determined by 3σ methods and were found to be 3.1 nM and 0.92 nM, respectively. The coordination modes of the complexes were investigated by computational and spectroscopic studies. Thus, the differentially selective turn-on fluorescence behavior of **H_3SAL-NH** for Zn^{2+} and Al^{3+} is based on a combined blocking of ESIPT and C=N isomerization, and chelation-enhanced fluorescence CHEF effects. *In vitro* cell imaging experiments showed that it can easily diffuse into the cell and can easily sense the Zn^{2+} and Al^{3+} ions by forming stable complexes at low concentrations.

Acknowledgements

Financial supports from CSIR (Ref. 02(2490)/11/EMR-II) and DST (Ref. SR/S1/IC-20/2012) New Delhi are gratefully acknowledged.

References

1 (*a*) A. Ajayaghosh, P. Carol and S. Sreejith, *J. Am. Chem. Soc.*, 2005, **127**, 14962; (*b*) J. W. Lee, H. S. Jung, P. S. Kwon, J. W. Kim, R. A. Bartsch, Y. Kim, S. Kim and J. S. Kim, *Org. Lett.*, 2008, **10**, 3801; (*c*) L. Xue, Q. Liu and H. Jiang, *Org. Lett.*, 2009, **11**, 3454; (*d*) J. F. Zhang, Y. Zhou, J. Yoon, Y. Kim, S. J. Kim and J. S. Kim, *Org. Lett.*, 2010, **12**, 3852; (*e*) J. F. Zhang, Y. Zhou, J. Yoon and J. S. Kim, *Chem. Soc. Rev.*, 2011, **40**, 3416.
2 D. Maity and T. Govindaraju, *Chem. Commun.*, 2012, **48**, 1039.
3 (*a*) S. Goswami, S. Paul and A. Manna, *RSC Adv.*, 2013, **3**, 25079; (*b*) S. Goswami, K. Aich, A. K. Das, A. Manna and S. Das, *RSC Adv.*, 2013, **3**, 2412.
4 H. X. Jiang, L. S. Chen, J. G. Zheng, S. Han, N. Tang and B. R. Smith, *Tree Physiol.*, 2008, **28**, 1863.
5 G. Berthon, *Coord. Chem. Rev.*, 1996, **149**, 241.
6 S. M. Candura, L. Manzo and L. G. Costa, Role of occupational neurotoxicants in psychiatric and neurodegenerative disorders, in *Occupational Neurotoxicology*, ed. L. G. Costa and L. Manzo, CRC Press, Boca Raton, 1998, pp. 131–167.
7 R. J. P. Williams, *Coord. Chem. Rev.*, 1992, **149**, 1.
8 G. R. Rout, S. S. Roy and P. Das, *Agronomie*, 2001, **21**, 3.
9 (*a*) J. Barcelo and C. Poschenrieder, *Environ. Exp. Bot.*, 2002, **48**, 75; (*b*) B. Valeur and I. Leray, *Coord. Chem. Rev.*, 2000,

205, 3; (*c*) Z. Krejpcio and R. W. P. Wojciak, *Int. J. Environ. Stud.*, 2002, **11**, 251.
10 M. R. Wills, C. D. Hewitt, B. C. Sturgill, J. Savory and M. M. Herman, *Ann. Clin. Lab. Sci.*, 1993, **23**, 1.
11 G. Sahin, I. Varol and A. Temizer, *Biol. Trace Elem. Res.*, 1994, **41**, 129.
12 A. C. Alfrey, *NeuroToxicology*, 1980, **1**, 43.
13 A. A. Buraimoh, S. A. Ojo, J. O. Hambolu and S. S. Adebisi, *Curr. Res. J. Biol. Sci.*, 2011, **3**, 509.
14 K. Soroka, R. S. Vithanage, D. A. Phillips, B. Walker and P. K. Dasgupta, *Anal. Chem.*, 1987, **59**, 629.
15 S. Das, M. Dutta and D. Das, *Anal. Methods*, 2013, **5**, 6262 and the references therein.
16 (*a*) E. Tomat and S. J. Lippard, *Inorg. Chem.*, 2010, **49**, 9113; (*b*) K. Komatsu, Y. Urano, H. Kojima and T. Nagano, *J. Am. Chem. Soc.*, 2007, **129**, 13447; (*c*) Y. Li, J. Wu, X. Jin, J. Wang, S. Han, W. Wu, J. Xu, W. Liu, X. Yao and Y. Tang, *Dalton Trans.*, 2014, **43**, 1881.
17 (*a*) K. R. Gee, Z. L. Zhou, D. Ton-That, S. L. Sensi and J. H. Weiss, *Cell Calcium*, 2002, **31**, 245; (*b*) K. R. Gee, Z. L. Zhou, W. J. Qian and R. Kennedy, *J. Am. Chem. Soc.*, 2002, **124**, 776; (*c*) E. J. Song, J. Kang, G. R. You, G. J. Park, Y. Kim, S.-J. Kim, C. Kim and R. G. Harrison, *Dalton Trans.*, 2013, **42**, 15514; (*d*) G. K. Tsikalas, P. Lazarou, E. Klontzas, S. A. Pergantis, I. Spanopoulos, P. N. Trikalitis, G. E. Froudakis and H. E. Katerinopoulos, *RSC Adv.*, 2014, **4**, 693; (*e*) Z. Liu, C. Zhang, Y. Chen, F. Qian, Y. Bai, W. He and Z. Guo, *Chem. Commun.*, 2014, **50**, 1253.
18 (*a*) B. Valeur, *Molecular Fluorescence Principles and Applications*, Wiley-VCH Verlag GmbH, New York, 2001, p. 341; (*b*) D. H. Vance and A. W. Czarnik, *J. Am. Chem. Soc.*, 1994, **116**, 9397; (*c*) S. K. Kim and J. Yoon, *Chem. Commun.*, 2002, 770.
19 (*a*) T. Gunnlaugsson, A. P. Davis, J. E. O'Brien and M. Glynn, *Org. Lett.*, 2002, **4**, 2449; (*b*) T. Mistri, R. Alam, M. Dolai, S. K. Mandal, A. R. Khuda-Bukhsh and M. Ali, *Org. Biomol. Chem.*, 2013, **11**, 1563; (*c*) R. Alam, T. Mistri, P. Mondal, D. Das, S. K. Mandal, A. R. Khuda-Bukhsh and M. Ali, *Dalton Trans.*, 2014, **43**, 2566.
20 (*a*) P. D. Beer, *Acc. Chem. Res.*, 1998, **31**, 71; (*b*) M. J. Kim, R. Konduri, H. Ye, F. M. MacDonnell, F. Puntoriero, S. Serroni, S. Campagna, T. Holder, G. Kinsel and K. Rajeshwar, *Inorg. Chem.*, 2002, **41**, 2471.
21 (*a*) Z. Xu, Y. Xiao, X. Qian, J. Cui and D. Cui, *Org. Lett.*, 2005, **7**, 889; (*b*) F. Y. Wu and Y. B. Jiang, *Chem. Phys. Lett.*, 2002, **355**, 438; (*c*) J. B. Wang, X. H. Qian and J. N. Cui, *J. Org. Chem.*, 2006, **71**, 4308.
22 (*a*) S. Nishizawa, Y. Kato and N. Teramae, *J. Am. Chem. Soc.*, 1999, **121**, 9463; (*b*) H. Yuasa, N. Miyagawa, T. Izumi, M. Nakatani, M. Izumi and H. Hashimoto, *Org. Lett.*, 2004, **6**, 1489; (*c*) B. Schazmann, N. Alhashimy and D. Diamond, *J. Am. Chem. Soc.*, 2006, **128**, 8607; (*d*) N. Chandrasekharan and L. A. Kelly, *J. Am. Chem. Soc.*, 2001, **123**, 9898; (*e*) J. S. Wu, J. H. Zhou, P. F. Wang, X. H. Zhang and S. K. Wu, *Org. Lett.*, 2005, **7**, 2133.
23 X. Zhang, L. Guo, F. Y. Wu and Y. B. Jiang, *Org. Lett.*, 2003, **5**, 2667.
24 V. C. da Silveira, J. S. Luz, C. C. Oliveira, I. Graziani, M. R. Ciriolo and A. M. D. C. Ferreira, *J. Inorg. Biochem.*, 2008, **102**, 1090.
25 (*a*) S. Padhye and G. B. Kauffman, *Coord. Chem. Rev.*, 1985, **63**, 127; (*b*) Y. Li and Z. Y. Yang, *Inorg. Chim. Acta*, 2009, **362**, 4823.
26 S. Kasselouri, A. Garoufis, A. Katehanakis, G. Kalkanis, S. P. Perlepes and N. Hadjiliadis, *Inorg. Chim. Acta*, 1993, **207**, 255; S. Padhye and G. B. Kauffman, *Coord. Chem. Rev.*, 1985, **63**, 127.
27 J. Wu, W. Liu, X. Zhuang, F. Wang, P. Wang, S. Tao, X. Zhang, S. Wu and S. T. Lee, *Org. Lett.*, 2007, **9**, 33.
28 M. Royzen, A. Durandin, V. G. Young, N. E. Geacintov and J. W. Canary, *J. Am. Chem. Soc.*, 2006, 128.
29 E. Lambert, B. Chabut, S. Chardon-Noblat, A. Deronzier, G. Chottard, A. Bousseksou, J. Tuchagues, J. Laugier, M. Bardet and J. M. Latour, *J. Am. Chem. Soc.*, 1997, **119**, 9424.
30 R. G. Parr and W. Yang, *Density Functional Theory of Atoms and Molecules*, Oxford University Press, Oxford, 1989.
31 (*a*) V. Barone and M. Cossi, *J. Phys. Chem. A*, 1998, **102**, 1995; (*b*) M. Cossi and V. Barone, *J. Chem. Phys.*, 2001, **115**, 4708; (*c*) M. Cossi, N. Rega, G. Scalmani and V. Barone, *J. Comput. Chem.*, 2003, **24**, 669.
32 A. D. Becke, *J. Chem. Phys.*, 1993, **98**, 5648.
33 C. Lee, W. Yang and R. G. Parr, *Phys. Rev. B: Condens. Matter Mater. Phys.*, 1998, **37**, 785.
34 (*a*) M. E. Casida, C. Jamoroski, K. C. Casida and D. R. Salahub, *J. Chem. Phys.*, 1998, **108**, 4439; (*b*) R. E. Stratmann, G. E. Scuseria and M. J. Frisch, *J. Chem. Phys.*, 1998, **109**, 8218; (*c*) R. Bauernschmitt and R. Ahlrichs, *Chem. Phys. Lett.*, 1996, **256**, 454.
35 (*a*) T. Liu, H.-X. Zhang and B.-H. Xia, *J. Phys. Chem. A*, 2007, **111**, 8724; (*b*) X. Zhou, H.-X. Zhang, Q.-J. Pan, B.-H. Xia and A.-C. Tang, *J. Phys. Chem. A*, 2005, **109**, 8809; (*c*) X. Zhou, A.-M. Ren and J.-K. Feng, *J. Organomet. Chem.*, 2005, **690**, 338; (*d*) A. Albertino, C. Garino, S. Ghiani, R. Gobetto, C. Nervi, L. Salassa, E. Rosenverg, A. Sharmin, G. Viscardi, R. Buscaino, G. Cross and M. Milanesio, *J. Organomet. Chem.*, 2007, **692**, 1377.
36 P. J. Hay and W. R. Wadt, *J. Chem. Phys.*, 1985, **82**, 299.
37 M. J. Frischet, *et. al.*, *Gaussian 09, (Revision A.1)*, Gaussian, Inc., Wallingford, CT, 2009.
38 N. M. O'Boyle, A. L. Tenderholt and K. M. Langner, *J. Comput. Chem.*, 2008, **29**, 839.
39 T. Mossman, *J. Immunol. Methods*, 1983, **65**, 55.
40 J. Zhao, S. Ji, Y. Chen, H. Guo and P. Yang, *Phys. Chem. Chem. Phys.*, 2012, **14**, 8803.
41 L. Wang, W. Qin, X. Tang, W. Dou and W. Liu, *J. Phys. Chem. A*, 2011, **115**, 1609.
42 J.-C. Qin, Z.-Y. Yang, L. Fan, X.-Y. Cheng, T.-R. Li and B.-D. Wang, *Anal. Methods*, 2014, **6**, 7343.
43 J. Karpagam, N. Sundaraganesan, S. Sebastian, S. Manoharan and M. Kurt, *J. Raman Spectrosc.*, 2010, **41**, 53.
44 R. Alam, T. Mistri, A. Katarkar, K. Chaudhuri, S. K. Mandal, A. R. Khuda-Bukhsh, K. K. Das and M. Ali, *Analyst*, 2014, **139**, 4022.

